~~CONFIDENTIAL~~

OFFICE OF SCIENTIFIC RESEARCH & DEVELOPMENT
NATIONAL DEFENSE RESEARCH COMMITTEE
DIVISION SIX - SECTION 6.1

FORCE TESTS OF THE SQUID WITH NEW AFTERBODY, TAILS, AND NOSES

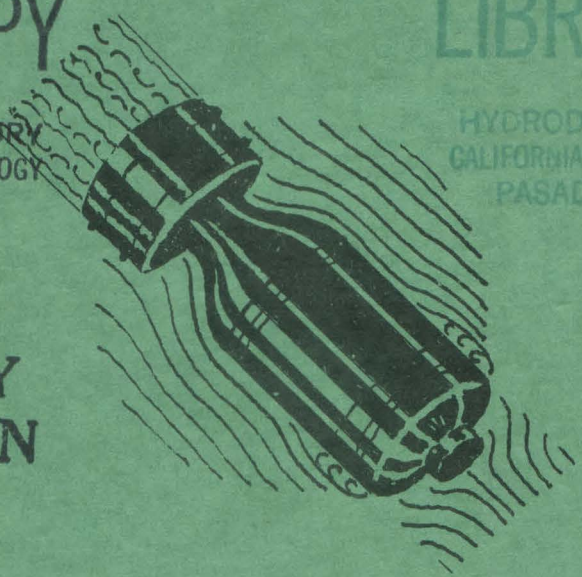

THE HIGH SPEED WATER TUNNEL
CALIFORNIA INSTITUTE OF TECHNOLOGY
PASADENA, CALIFORNIA

SECTION Nº 6.1-sr 207-2243
LABORATORY Nº ND-24.3

~~CONFIDENTIAL~~

OFFICE OF SCIENTIFIC RESEARCH AND DEVELOPMENT
NATIONAL DEFENSE RESEARCH COMMITTEE
DIVISION SIX — SECTION 6.1

FORCE TESTS OF THE SQUID WITH NEW AFTERBODY, TAILS, AND NOSES

ROBERT T. KNAPP
OFFICIAL INVESTIGATOR

THE HIGH SPEED WATER TUNNEL
AT THE
CALIFORNIA INSTITUTE OF TECHNOLOGY
HYDRODYNAMICS LABORATORY
PASADENA, CALIFORNIA

Section No. 6.1-sr207-2243

Laboratory No. ND-24.3

Report Prepared by
Gerald B. Robison
Hydraulic Engineer

July 30, 1945

SUMMARY AND CONCLUSIONS

Various modifications of the external shape, but not of overall length or diameter, of the British Squid, Type "C" Projectile were tested to determine an acceptable shape having materially reduced drag and no other characteristics which would be objectionable.

The best modification obtained was the simple substitution of a special nose, previously designed by Mr. A. L. Kitselman, who was then employed by the Hydrodynamics Laboratory. The contour of this special nose was determined by the formula $(X/1.5)^3 + Y^2 = 1$. This model appears, by extrapolation, to have a drag coefficient of about 0.106 at $R = 15 \times 10^6$ which would correspond to a terminal velocity of about 53.6 ft/sec. Calculations indicate that this might be raised to 55.0 by using four (strengthened) vanes in the tail instead of eight. The cross force coefficient is about 10% less than that of the production model, and the stabilizing moment coefficient about 11-1/2% greater. It is believed a bourrelet could be provided without materially affecting the hydrodynamic characteristics. The tendency to cavitate with this nose is somewhat reduced but its effect on performance during the bubble stage is not known at present, or even that it may be adverse. If so, it is probable that it could be within acceptable limits.

CONCLUSIONS

1. The drag coefficient appears reducible to approximately 0.106 at $R = 15 \times 10^6$ by the substitution of the special nose described herein.

2. Further reduction may be obtained by the use of a four-vane tail.

3. No objectionable characteristics appear to be introduced by the special nose with the possible exception of an unknown effect due to reduced cavitation in the bubble stage during water entry.

4. Further drag reduction appears feasible by improvements in the afterbody and tail design.

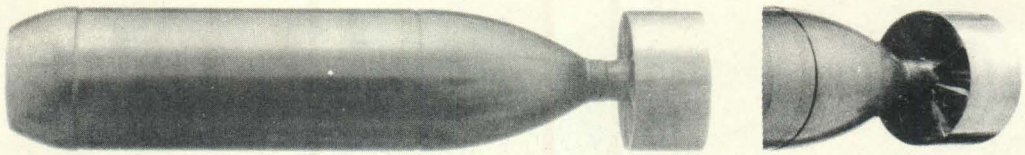

(A) PROTOTYPE WITH 8-VANE TAIL

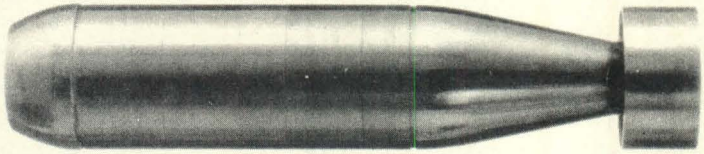

(B) CONE AFTERBODY, 4-VANE TAIL

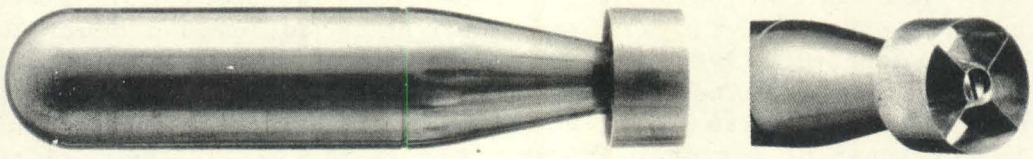

(C) HEMISPHERICAL NOSE, 4-VANE TAIL

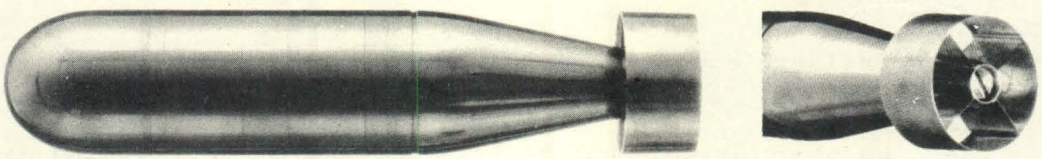

(D) SPECIAL NOSE, CONE TAIL

FIG. 1 – VIEWS OF BASIC SQUID MODIFICATIONS TESTED

FORCE TESTS OF THE BRITISH SQUID WITH NEW AFTERBODY, TAILS, AND NOSES

PURPOSE OF TESTS

The tests reported herein were made to determine acceptable modifications of the production model of the British Squid, Type "C" Projectile, which would reduce the drag materially and hence increase the terminal velocity.

AUTHORIZATION

Authorization to make these tests in the Water Tunnel of the Hydrodynamics Laboratory at the California Institute of Technology is contained in a letter of November 1, 1944, from Dr. E. H. Colpitts, Chief of Section 6.1, Office of Scientific Research and Development.

SUMMARY OF PROTOTYPE DATA

The production model of this depth charge, also referred to as the prototype, had these characteristics:

Overall length	55 inches = 4.583 ft.
Maximum diameter	11.9 inches
Maximum cross-sectional area perpendicular to the longitudinal axis, A_D	.0.772 sq. ft.
Weight, in air	386.4 pounds
in sea water	234 pounds

The appearance of the prototype (or production) model is shown in Figure 1 (A), and its outline drawing in Figure 2.

MODIFICATIONS

A simple new afterbody, shown in Figure 1 (B) to (D) inclusive, and in the outline in Figure 2, was designed to eliminate the turbulence which appeared to exist at the rear of the prototype afterbody. As may be seen, it consists, in effect, of a cone tangent to the original afterbody and with a truncated diameter equal to that of the original boom at the extreme rear end of the projectile.

Two new tails were made which were like the prototype tails except that both had only four radial fins instead of eight, and

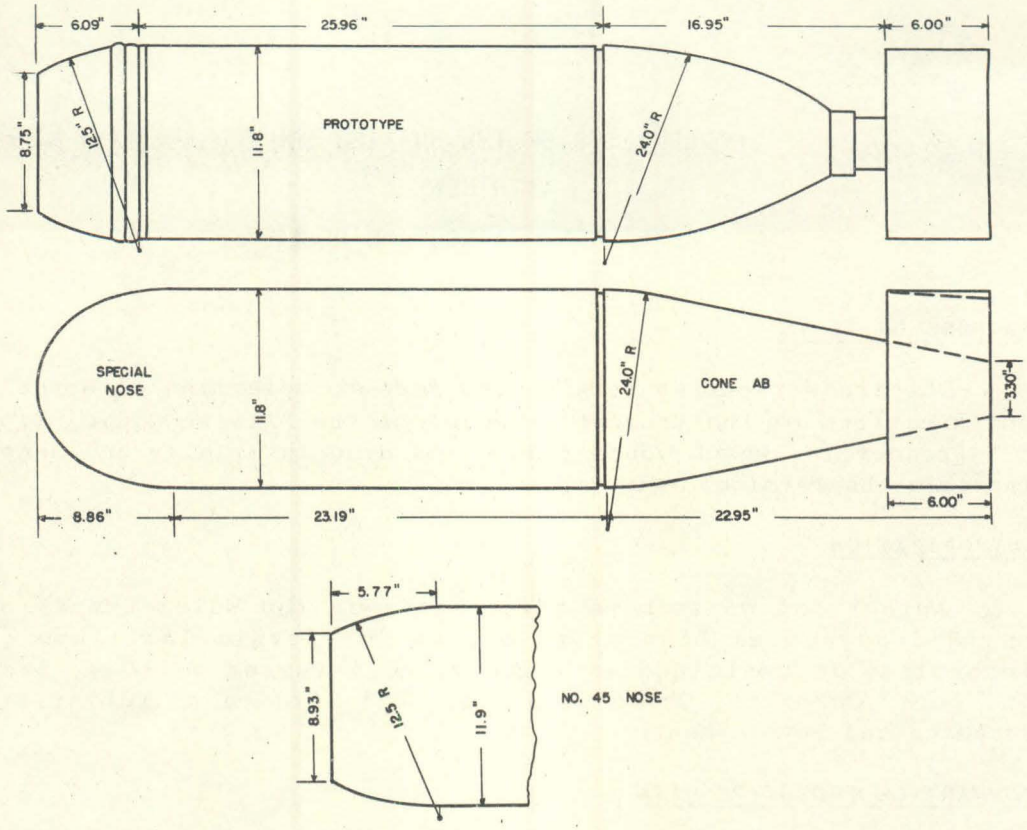

FIG. 2 – OUTLINE DRAWING

one had a cone angle* of 2° instead of 0°. Tail fin and ring thickness in the model were 0.012 and 0.015, respectively, equivalent to 0.07 and 0.089 in the prototype. The ring thickness of the prototype is actually 0.08. The difference was introduced to match the ring thickness of the existing prototype model. Leading edges of fins and rings were rounded. These tails, as constructed, included that portion of the afterbody which was within the tail length. The four-vane cylindrical tail is shown in Figure 1 (C), and the four-vane 2° cone tail in Figure 1 (D).

Two other noses, in addition to the prototype nose, were used in the tests. One was a simple hemisphere, shown in Figure 1 (C), and the other was a special nose having a contour based on the formula $(X/1.5)^3 + Y^2 = 1$. The length of the contoured portion is 1.5 times the radius. Table I gives the data for a unity radius nose of this shape. The nose may be seen in Figure 1 (D) and in the outline in Figure 2. See Table I for contour points based on unity radius.

*The cone angle, as used herein, is the angle formed, in any plane section which includes the longitudinal axis, by the intersection of the cone sides at the vertex.

While the two new tails could be used only with the new afterbody, all other parts were interchangeable, which permitted numerous combinations for test purposes.

TABLE I

Contour Points for Nose with Equation $\left(\frac{X}{1.5}\right)^3 + Y^2 = 1$

'L	R	'L	R	'L	R	'L	R
0	1.0000	0.9449	0.8660	1.1906	0.7071	1.3628	0.5000
0.3232	0.9950	0.9574	0.8602	1.1984	0.7000	1.3689	0.4899
0.4072	0.9899	0.9695	0.8544	1.2062	0.6928	1.3748	0.4796
0.4661	0.9849	0.9813	0.8485	1.2139	0.6855	1.3808	0.4690
0.5130	0.9798	0.9929	0.8426	1.2215	0.6782	1.3867	0.4582
0.5526	0.9747	1.0041	0.8366	1.2290	0.6708	1.3925	0.4472
0.5872	0.9695	1.0152	0.8306	1.2364	0.6633	1.3983	0.4359
0.6182	0.9643	1.0260	0.8246	1.2437	0.6557	1.4040	0.4242
0.6463	0.9591	1.0366	0.8185	1.2509	0.6480	1.4097	0.4123
0.6722	0.9539	1.0469	0.8124	1.2581	0.6403	1.4153	0.4000
0.6962	0.9487	1.0571	0.8062	1.2651	0.6324	1.4209	0.3873
0.7187	0.9434	1.0671	0.8000	1.2721	0.6245	1.4265	0.3741
0.7399	0.9381	1.0769	0.7937	1.2791	0.6164	1.4320	0.3605
0.7599	0.9327	1.0865	0.7874	1.2859	0.6083	1.4374	0.3464
0.7789	0.9273	1.0959	0.7810	1.2927	0.6000	1.4429	0.3316
0.7970	0.9219	1.1052	0.7746	1.2994	0.5916	1.4482	0.3162
0.8142	0.9165	1.1143	0.7681	1.3060	0.5831	1.4536	0.3000
0.8309	0.9110	1.1233	0.7616	1.3126	0.5744	1.4589	0.2828
0.8469	0.9055	1.1322	0.7550	1.3190	0.5657	1.4642	0.2646
0.8623	0.9000	1.1409	0.7483	1.3255	0.5568	1.4694	0.2449
0.8772	0.8944	1.1495	0.7416	1.3319	0.5477	1.4746	0.2236
0.8916	0.8888	1.1579	0.7348	1.3382	0.5385	1.4797	0.2000
0.9055	0.8832	1.1662	0.7280	1.3444	0.5291	1.4848	0.1732
0.9190	0.8775	1.1745	0.7211	1.3506	0.5196	1.4899	0.1414
0.9322	0.8718	1.1862	0.7141	1.3568	0.5099	1.4950	0.1000
						1.5000	0.0000

R = radius of cross section, inches

'L = distance along longitudinal axis from last unit radius, inches

'Table based on R = 1

TESTS MADE

All models had the same overall length and support point which was located at the center of gravity of the prototype.

Tests were intended to disclose the influence of the various parts upon the characteristic performance of the whole, but with particular emphasis on the drag coefficient.

The tests made included the determination of the amount and variation of the drag coefficient, C_D*, with Reynolds number; the amount and variation of the drag, cross force, and moment coefficients, C_D, C_C, and C_M for yaw angles between 0° and 10°, inclusive; flow diagrams which were obtained in the Polarized Light Flume; and some cavitation measurements and photographs.

RESULTS OBTAINED AND DISCUSSION

Figure 3 shows the relationship of the drag coefficient and Reynolds number for the two groups -- cylindrical (0°) tails and cone angle (2°) tails. All curves pertain to models with the new cone afterbody except the lowest curve of the upper group, which is for the special nose on the otherwise full prototype body. Observations were made to R = 4 x 10^6 and the lines were extrapolated to full scale R, calculated as approximately 15 x 10^6 for sea water at an average temperature of 50° Fahrenheit and a terminal velocity of 45 fps.

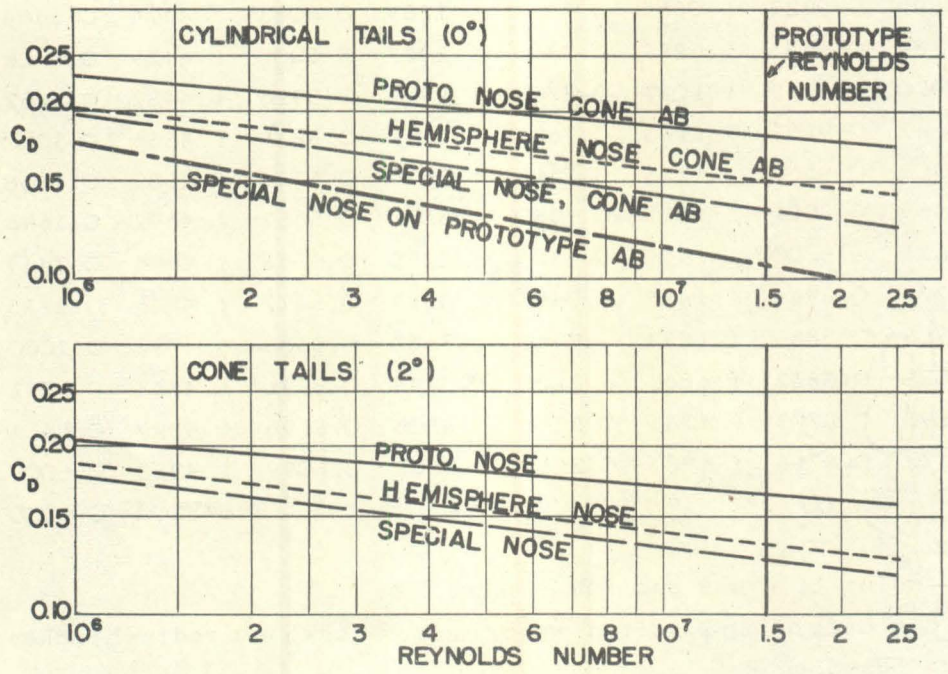

FIG. 3 – DRAG COEFFICIENT AGAINST REYNOLDS NUMBER

* See Appendix for definitions of symbols

Tests were to determine amounts and variations of the force coefficients with the modifications. It was natural to expect the drag coefficient to be less with the hemisphere and special noses than with the blunt prototype nose. This trend is to be seen in both groups. When other things are equal, the drag coefficient is less, at given R, with the 2° tails than those of 0°. This is due to a better fit to the flow lines over the conical afterbody. The prototype model was not tested with a 2° tail since none suitable was available. However, investigations indicated that the cylindrical ring is (or is near) an optimum for the prototype afterbody.

TABLE II

C_D for Various Models at R = 15 x 10^6

	0° Tail	Terminal Velocity	2° Tail	Terminal Velocity
Prototype nose, cone afterbody	0.180	41.3	0.165	43.0
Hemisphere nose, cone afterbody	0.150	45.1	0.134	47.7
Special nose, cone afterbody	0.133	47.9	0.125	49.4
Special nose on prototype	0.106	53.6		

The terminal velocity of the production model was previously calculated to be about 45 ft/sec, and was so reported in Report No. 6.1-sr207-1904, "Drag Tests of the British Squid," January 8, 1945. The value of 53.6 ft/sec here predicted from extrapolation of the line for the prototype with special nose, is an increase of approximately 20%. This was the eight-vane tail. The total area of both sides of four vanes is about 7-1/2% of the total wetted surface. Assuming that the skin friction is proportional to this wetted area, it would be reduced that much by their removal. Assuming also that the skin friction coefficient is the same as a flat plate of the same surface and length, (Karman "Turbulence and Skin Friction," J. Ae. Sc., Vol. I, No. 1, January, 1934) it would be 0.064 at R = 15 x 10^6. Seven and one-half per cent of this is about 0.005, giving a reduction of the *total* drag coefficient from 0.106 to 0.101. This would correspond to a terminal velocity of 55.0 ft/sec.

It may be noted also that, in general, an improvement in nose shape (while other parts are unchanged) has a double advantage. The drag coefficient is reduced at a given R because of the reduced form drag but, in addition, there is a greater percentage reduction at the higher Reynolds numbers. This latter effect is contrary to that obtained from tests of the Mk 13-1 Torpedo with various noses (Report Section No. 6.1-sr207-1909, February 1, 1945). The explanation is believed to be somewhat as follows.

Granted a perfect afterbody and tail structure, the form drag coefficient for those parts would have an absolute minimum. Form drag improvement would be confined to, and depend upon, the

nose shape. A blunt nose will have a relatively high form drag and, hence, greater opportunity for reduction of this drag at higher Reynolds numbers. On the other hand, finer noses, producing less turbulence, have less opportunity to improve at higher velocities. The Mk 13-1 Torpedo afterbody has a low form drag compared to that of the Squid afterbody, hence the effects are akin to those produced by the perfect afterbody and tail. When a fine nose is used with the Squid afterbody and tail, the nose form drag is decreased, but there is also a greater opportunity for the reduction of the separation (which exists around this afterbody) at high Reynolds numbers.

Table III shows the relative percentage which is attributable to form drag at $R = 1 \times 10^6$ and 15×10^6 for the models tested. These figures were obtained from calculations of the equivalent flat plate skin friction coefficient, based on the work of Karman, previously cited. The form drag coefficient was taken as the remainder after subtracting this skin friction coefficient from the total drag coefficient.

TABLE III

Percentage Relationship of Form Drag Coefficient to Total Drag Coefficient

0° Tails	$R = 10^6$	$R = 15 \times 10^6$	Change
Prototype nose, cone afterbody	57.5%	64.0%	+6.5%
Hemisphere nose, cone afterbody	51.5	57.5	+6.0
Special nose, cone afterbody	49.5	51.4	+1.9
Special nose, prototype afterbody	42.7	40.0	-2.7
2° Tails			
Prototype nose, cone afterbody	51.5	60.0	+8.5
Hemisphere nose, cone afterbody	46.2	52.4	+6.2
Special nose, cone afterbody	43.0	48.5	+5.5

Figure 4 presents the influence of yaw angle on the drag and cross force coefficients for the various models tested. The lines, as well as those in Figures 3 and 5, are representative as follows:

Solid lines	Prototype nose, cone afterbody, 0° and 2° tails
Short dash	Hemisphere nose, cone afterbody, 0° and 2° tails
Long dash	Special nose, cone afterbody, 0° and 2° tails
Dash-dot	Special nose, prototype afterbody
Dash-two dots	Early Squid model with nose most nearly like that of the production model (for which no such data were available)

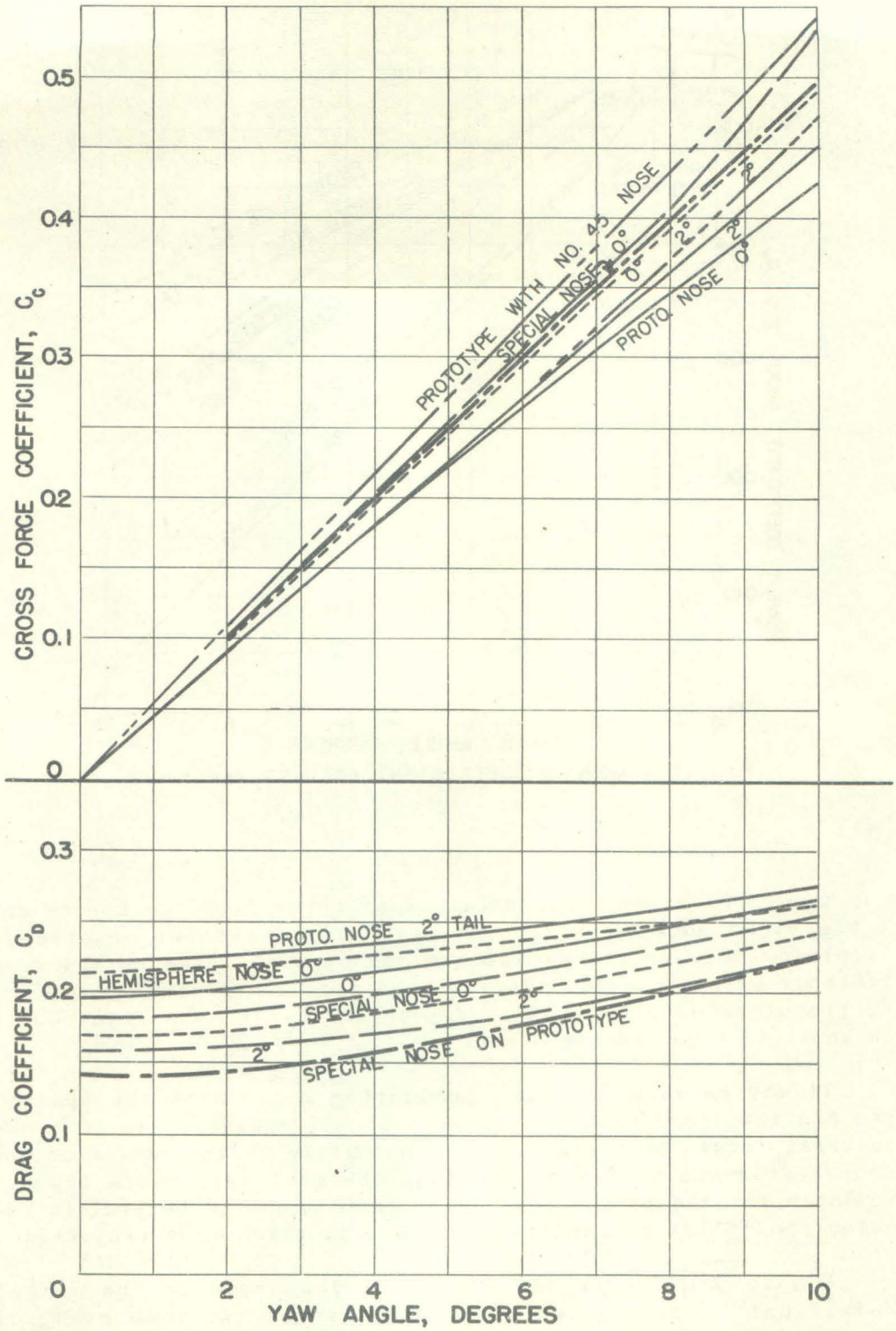

FIG. 4 – DRAG AND CROSS FORCE COEFFICIENTS AGAINST YAW ANGLE

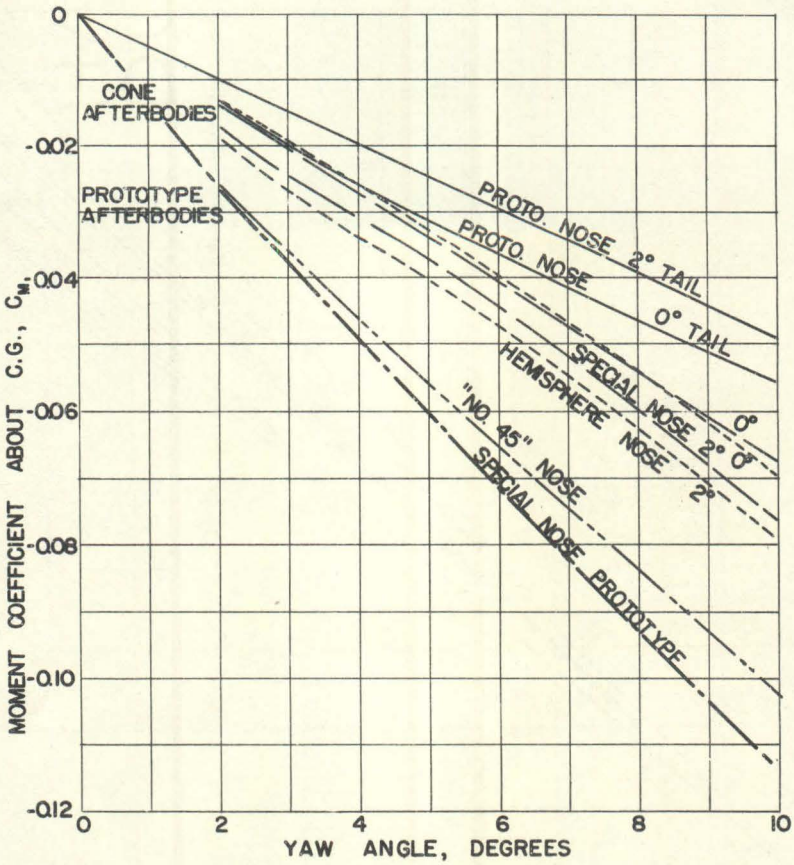

FIG. 5 – MOMENT COEFFICIENT AGAINST YAW ANGLE

The third cross force coefficient curve from the bottom and at the right edge is a doublet which represents no observable difference between the hemisphere and special noses on the cone afterbody with 2° tails. There is no drag coefficient curve for the prototype with "No. 45" nose, as that which was obtained is now known to have been in error.

It may be seen that the production model with the special nose has the least drag coefficient at all angles up to 10°, and its cross force coefficient is approximately in the center of the group tested and some 10% less than the most applicable figures available for the production model. This might be helpful in reducing the "planing" tendency of the production type projectile.

Figure 5 presents the effect of yaw angle on the moment coefficient about the center of gravity for the same group of models. The static stability of the prototype model with special nose is not only greater than that of any other modification tested, but is 11.1/2% greater at 10° yaw than the model approximating the production type.

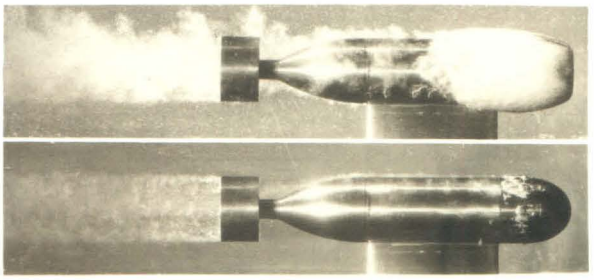

PROTOTYPE

PROTOTYPE WITH SPECIAL NOSE

K = 0.45

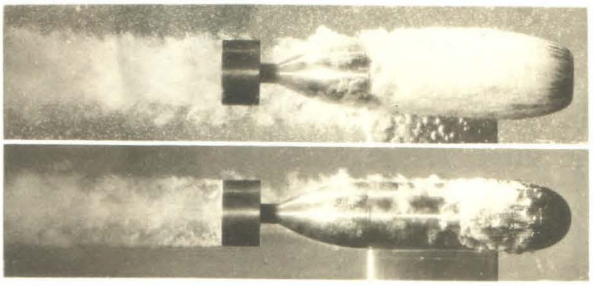

PROTOTYPE

PROTOTYPE WITH SPECIAL NOSE

K = 0.35

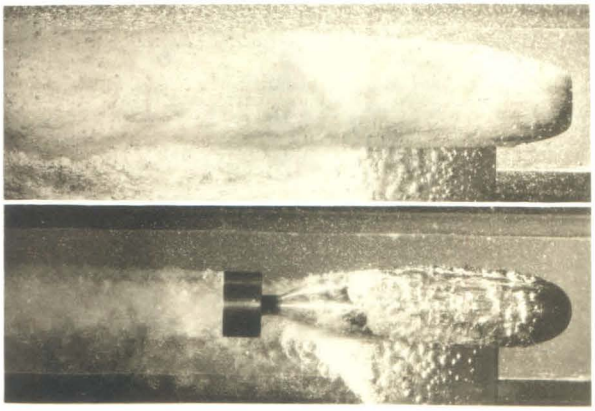

PROTOTYPE

PROTOTYPE WITH SPECIAL NOSE

K = 0.25

FIG. 6 – CAVITATION WITH PROTOTYPE AND PROTOTYPE WITH SPECIAL NOSE

Figure 6 shows comparative cavitation effects for the production model and the same model with special nose substituted, for K values of 0.45, 0.35, and 0.25. The cavitation is, of course, less for the smoother nose, but the difference is not enormous. The exact influence of this nose during the bubble stage is not known at present. It is not certain that its effect would be adverse to the action desired therein and, if it were, it is probable that it would be within acceptable limits.

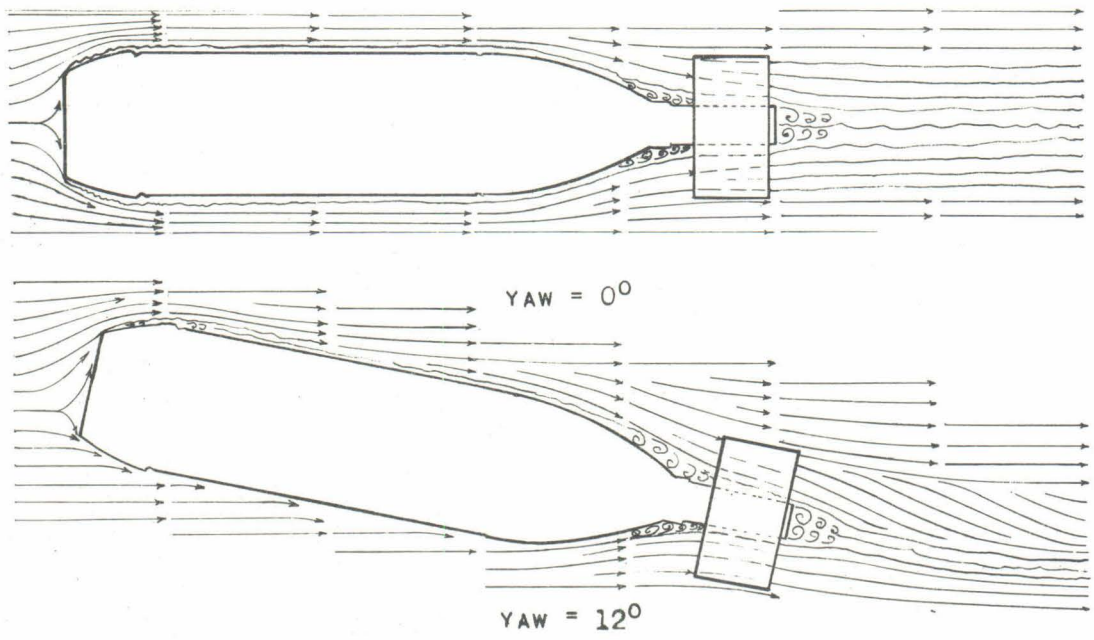

FIG. 7

Fig. 7 is the flow diagram for the production model at 0° and 12° yaw. The disturbance due to separation around the afterbody, previously mentioned, is apparent.

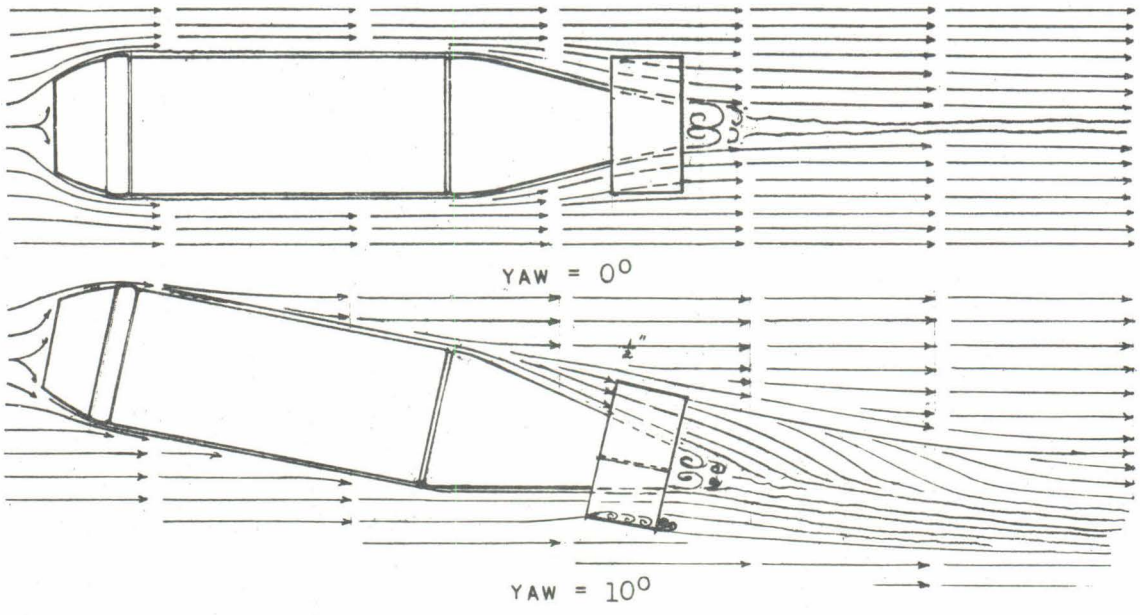

FIG. 8

Fig. 8 is a flow diagram for the model with prototype nose, cone afterbody, and 0° tail. Separation around this afterbody does not occur, but the test results seem to indicate that its elimination produced little advantage in total drag reduction.

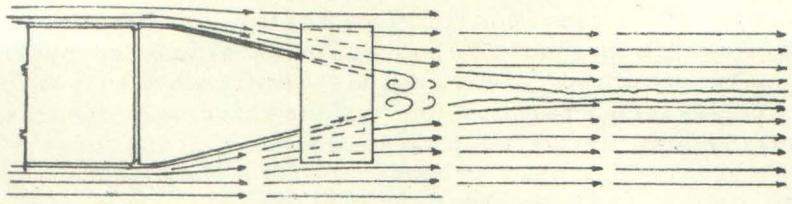

YAW = 0°

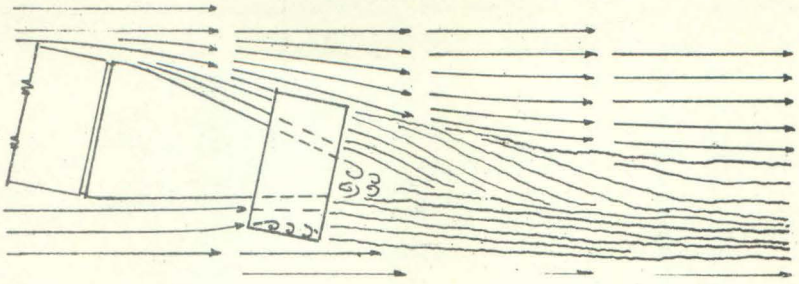

YAW = 10°

FIG. 9

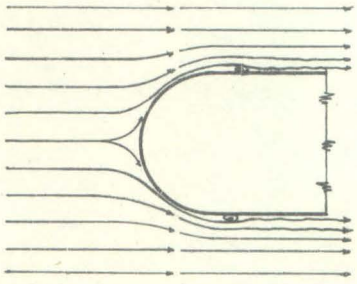

FIG. 10

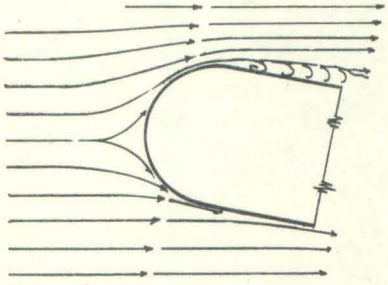

FIG. 11

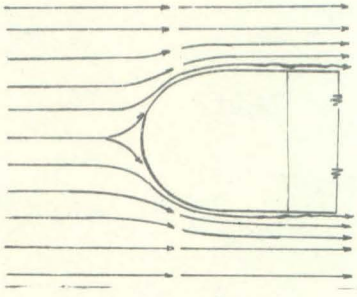

FIG. 12

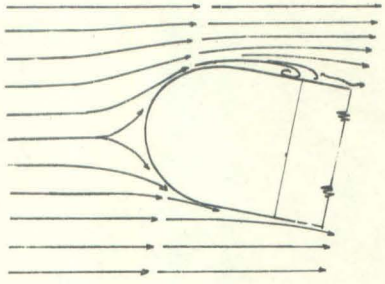

FIG. 13

Figure 9 is the flow diagram for the cone afterbody and 2° tail; Figures 10 and 11, for the hemisphere nose at 0° and 10° yaw; and Figures 12 and 13 for the special nose at 0° and 10° yaw.

Figure 9 gives an indication of better tail fit to the flow through it. Figures 10, 11, 12, and 13 show progressively reduced the tendency for the flow to separate from the body at 0° and 10° yaw angles when compared to the prototype nose.

The field of investigation for further reduction of drag coefficient for this projectile has not been exhausted by the modifications here reported. The conical afterbody did not provide the reduction desired, perhaps due to insufficient open area between the afterbody and ring at the forward plane of the ring. Further investigation should produce an afterbody and a tail with proper cone angle that would reduce this drag still further.

APPENDIX

DEFINITIONS

YAW ANGLE, ψ

The angle, in a horizontal plane, which the axis of the projectile makes with the direction of motion. Looking down on the projectile, yaw angles in a clockwise direction are positive (+) and in a counterclockwise direction, negative (−).

PITCH ANGLE, α

The angle, in a vertical plane, which the axis of the projectile makes with the direction of motion. Pitch angles are positive (+) when the nose is up and negative (−) when the nose is down.

LIFT, L

The force, in pounds, exerted on the projectile normal to the direction of motion and in a vertical plane. The lift is positive (+) when acting upward and negative (−) when acting downward.

CROSS FORCE, C

The force, in pounds, exerted on the projectile normal to the direction of motion and in a horizontal plane. The cross force is positive when acting in the same direction as the displacement of the projectile nose for a positive yaw angle, i.e., to an observer facing in the direction of travel, a positive cross force acts to the right.

DRAG, D

The force, in pounds, exerted on the projectile parallel with the direction of motion. The drag is positive when acting in a direction opposite to the direction of motion.

MOMENT, M

The torque, in foot pounds, tending to rotate the projectile about a transverse axis. Yawing moments tending to rotate the projectile in a clockwise direction (when looking down on the projectile) are positive (+), and those tending to cause counterclockwise rotation are negative (−). Pitching moments tending to rotate the projectile in a clockwise direction (when looking at the projectile from the port side) are positive (+), and those tending to cause counterclockwise rotation are negative (−).

In accordance with this sign convention a moment has a destabilizing effect when it has the same sign as the yaw angle or pitch angle, and a stabilizing effect when the moment and yaw or pitch angle have opposite signs

NORMAL COMPONENT, N

The sum of the components of the drag and cross force (or lift) acting normal to the axis of the projectile. The value of the normal component is given by the following:

$$N = D \sin \psi + C \cos \psi \qquad (1)$$

or

$$N = D \sin \alpha + L \cos \alpha \qquad (1a)$$

in which

N = Normal component in lbs

D = Drag in lbs

C = Cross force in lbs

L = Lift force in lbs

ψ = Yaw angle in degrees

α = Pitch angle in degrees

CENTER OF PRESSURE, CP

The point in the axis of the projectile at which the resultant of all forces acting on the projectile is applied.

CENTER-OF-PRESSURE ECCENTRICITY, e

The distance between the center of pressure (CP) and the center of gravity (CG) expressed as a decimal fraction of the length (l) of the projectile. The center-of-pressure eccentricity is derived as follows:

$$e = (l_{cp} - l_{cg}) \frac{1}{l} = \frac{1}{l} \frac{M_{cg}}{N} \qquad (2)$$

in which

e = Center-of-pressure eccentricity

l = Length of projectile in feet

l_{cg} = Distance from nose of projectile to CG in feet

l_{cp} = Distance from nose of projectile to CP in feet

COEFFICIENTS

The force and moment coefficients used are derived as follows:

Drag coefficient, $$C_D = \frac{D}{\rho \frac{V^2}{2} A_D} \quad (3)$$

Cross force coefficient, $$C_C = \frac{C}{\rho \frac{V^2}{2} A_D} \quad (4)$$

Lift coefficient, $$C_L = \frac{L}{\rho \frac{V^2}{2} A_D} \quad (5)$$

Moment coefficient, $$C_M = \frac{M}{\rho \frac{V^2}{2} A_D l} \quad (6)$$

in which

D = Measured drag force in lbs

C = Measured cross force in lbs

L = Measured lift force in lbs

ρ = Density of the fluid in slugs/cu ft = w/g

w = Specific weight of the fluid in lbs/cu ft

g = Acceleration of gravity in ft/sec^2

A_D = Area in sq ft at the maximum cross section of the projectile taken normal to the geometric axis of the projectile

V = Mean relative velocity between the water and the projectile in ft/sec

M = Moment, in foot-pounds, measured about any particular point on the geometric axis of the projectile

l = Overall length of the projectile in feet

RUDDER EFFECT

The total increase or decrease in moment coefficient, at a given yaw or pitch angle, resulting from a given rudder setting. This increase or decrease in moment coefficient is measured from the moment coefficient curve for neutral rudder setting.

REYNOLDS NUMBER

In comparing hydraulic systems involving only friction and inertia forces, a factor called Reynolds number is of great utility. This is defined as follows:

$$R = \frac{lV}{\nu} = \frac{lV\rho}{\mu} \qquad (7)$$

in which

R = Reynolds number

l = Overall length of projectile, feet

V = Velocity of projectile, feet per sec

ν = Kinematic viscosity of the fluid, sq ft per sec = μ/ρ

ρ = Mass density of the fluid in slugs per cu ft

μ = Absolute viscosity in pound-seconds per sq ft

Two geometrically similar systems are also dynamically similar when they have the same value of Reynolds number. For the same fluid in both cases, a model with small linear dimensions must be used with correspondingly large velocities. It is also possible to compare two cases with widely differing fluids provided l and V are properly chosen to give the same value of R.

CAVITATION PARAMETER

In the analysis of cavitation phenomena, the cavitation parameter has been found very useful. This is defined as follows:

$$K = \frac{P_L - P_B}{\rho \frac{V^2}{2}} \qquad (8)$$

in which

K = Cavitation parameter

P_L = Absolute pressure in the undisturbed liquid, lbs/sq ft

P_B = Vapor pressure corresponding to the water temperature, lbs/sq ft

V = Velocity of the projectile, ft/sec

ρ = mass density of the fluid in slugs per cu ft = w/g

w = weight of the fluid in lbs per cu ft

g = acceleration of gravity

Note that any homogeneous set of units can be used in the computation of this parameter. Thus, it is often convenient to express this parameter in terms of the head, i.e.,

$$K = \frac{h_L - h_B}{\frac{V^2}{2g}} \qquad (9)$$

where

h_L = Submergence plus the barometric head, ft of water

h_B = Pressure in the bubble, ft of water

It will be seen that the numerator of both expressions is simply the net pressure acting to collapse the cavity or bubble. The denominator is the velocity pressure. Since the entire variation in pressure around the moving body is a result of the velocity, it may be considered that the velocity head is a measure of the pressure available to open up a cavitation void. From this point of view, the cavitation parameter is simply the ratio of the pressure available to collapse the bubble to the pressure available to open it. If the K for incipient cavitation is considered, it can be interpreted to mean the maximum reduction in pressure on the surface of the body measured in terms of the velocity head. Thus, if a body starts to cavitate at the cavitation parameter of one, it means that the lowest pressure at any point on the body is one velocity head below that of the undisturbed fluid.

The shape and size of the cavitation bubbles for a specific projectile are functions of the cavitation parameter. If p_B is taken to represent the gas pressure within the bubble instead of the vapor pressure of the water, as in normal investigations, the value of K obtained by the above formula will be applicable to an air bubble. In other words, the behavior of the bubble will be the same whether the bubble is due to cavitation, the injection of exhaust gas, or the entrainment of air at the time of launching.

The cavitation parameter for incipient cavitation has the symbol K_i.

The following chart gives values of the cavitation parameter as a function of velocity and submergence in sea water.

GENERAL DISCUSSION OF STATIC STABILITY

Water tunnel tests are made under steady flow conditions, consequently the results only indicate the tendency of the steady state hydrodynamic couples and forces to cause the projectile to return to or move away from its equilibrium position after a

disturbance. Dynamic couples and forces including either positive or negative damping are not obtained. If the hydrodynamic moments are restoring the projectile, then it is said to be statically stable, if nonrestoring, statically unstable. In the discussion of static stability the actual motion following a perturbation is not considered at all. In fact, the projectile may oscillate continuously about an equilibrium position without remaining in it. In this case it would be statically stable, but would have zero damping and hence, be dynamically unstable. With negative damping a projectile would oscillate with continually increasing amplitude following an initial perturbation even though it were statically stable. Equilibrium is obtained if the sum of the hydrodynamic, buoyant, and propulsive moments equal zero. In general, propulsive thrusts act through the center of gravity of the projectile so only the first two items are important.

If a projectile is rotating from its equilibrium position so as to increase its yaw angle positively, the moment coefficient must increase negatively (according to the sign convention adopted) in order that it be statically stable. Therefore, for projectiles without controls or with fixed control surfaces, a negative slope of the curve of moment coefficient vs yaw gives static stability and a positive slope gives instability. For a projectile without controls, static stability is necessary for a successful flight unless stability is obtained by spinning as in the case of rifle shells. For a projectile with controls, stabilizing moments can be obtained by adjusting the control surfaces, and the slope of the moment coefficient, as obtained with fixed rudder position, need not give static stability. Where buoyancy either acts at the center of gravity or can be neglected, equilibrium is obtained when the hydrodynamic moment coefficient equals zero. For symmetrical projectiles this occurs at zero yaw angle, i.e., when the projectile axis is parallel to the trajectory. For nonsymmetrical projectiles, such as a torpedo when the rudders are not neutral, the moment is not zero at zero yaw but vanishes at some definite angle of attack. Where buoyancy cannot be neglected equilibrium is obtained when $C_M = -C_{Buoyancy}$, and the axis of the projectile is at some angle with the trajectory.

For symmetrical projectiles the degree of stability or instability can be obtained from the center of pressure curves. If the center of pressure falls behind the center of gravity, a restoring moment exists giving static stability. If the center of pressure falls ahead of the center of gravity, the moment is nonrestoring, and the projectile will be statically unstable. The degree of stability or instability is indicated approximately by the distance between the center of gravity and the center of pressure. In general, for nonsymmetrical projectiles, the cross force or lift is not zero when the moment vanishes so that the center of pressure curve is not symmetrical and the simple rules just stated cannot be used to determine whether or not the projectile will be stable. In such cases careful interpretation of the moment curves is a more satisfactory method of determining stability relationship.

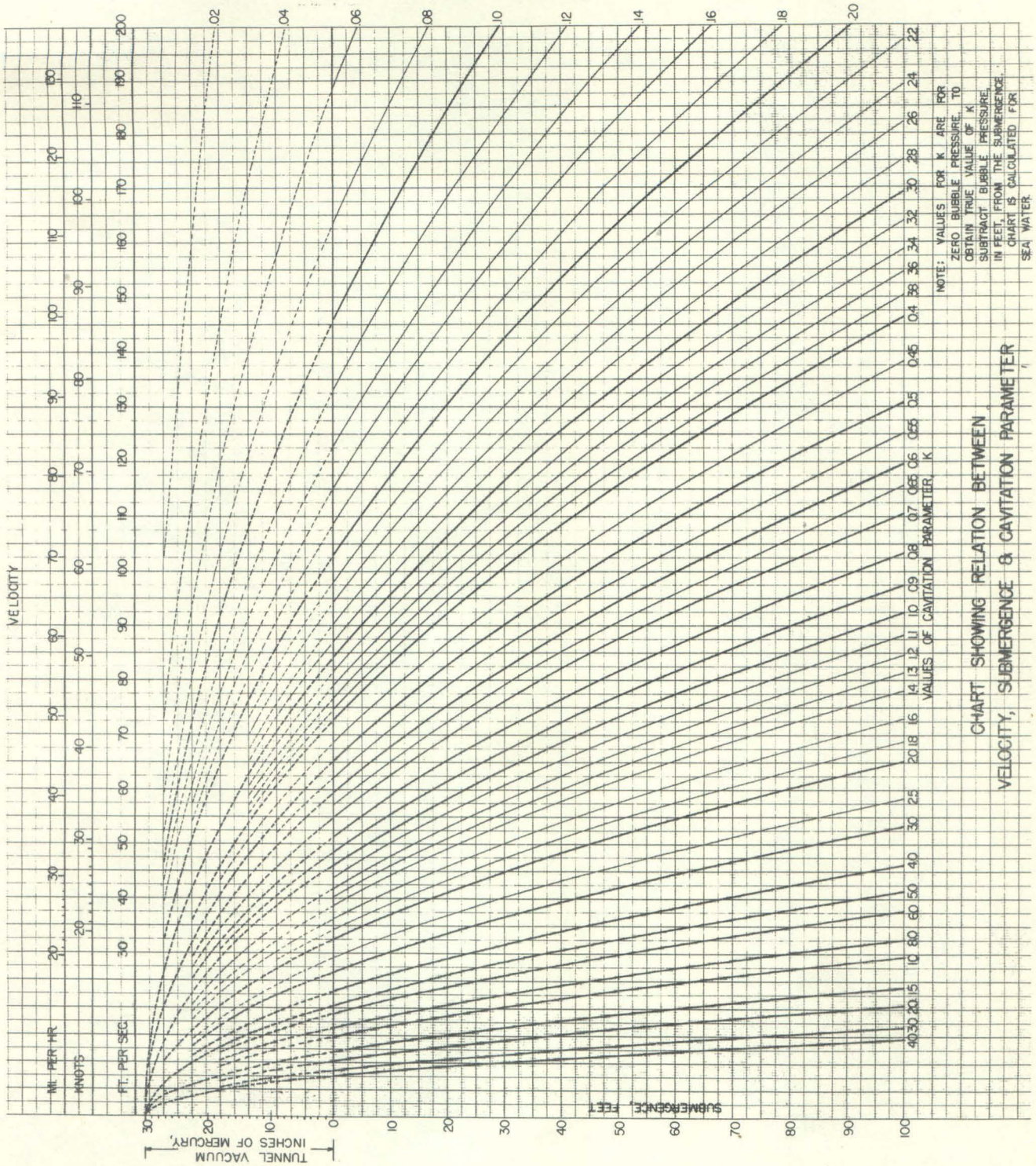
CHART SHOWING RELATION BETWEEN
VELOCITY, SUBMERGENCE & CAVITATION PARAMETER
NOTE: VALUES FOR K ARE FOR ZERO BUBBLE PRESSURE. TO OBTAIN TRUE VALUE OF K SUBTRACT BUBBLE PRESSURE IN FEET, FROM THE SUBMERGENCE. CHART IS CALCULATED FOR SEA WATER.
VALUES OF CAVITATION PARAMETER, K
SUBMERGENCE, FEET
TUNNEL VACUUM INCHES OF MERCURY,
VELOCITY
MI. PER HR.
KNOTS
FT. PER SEC.